Title
A Feasibility Study Showing [68Ga]Citrate PET Detects Prostate Cancer

Journal
Molecular Imaging and Biology, 18(6)

ISSN
1536-1632

Authors
Behr, Spencer C
Aggarwal, Rahul
Seo, Youngho
et al.

Publication Date
2016-12-01

DOI
10.1007/s11307-016-0966-5

Peer reviewed

HHS Public Access

Author manuscript

Mol Imaging Biol. Author manuscript; available in PMC 2019 March 22.

Published in final edited form as:

Mol Imaging Biol. 2016 December ; 18(6): 946–951. doi:10.1007/s11307-016-0966-5.

A feasibility study showing [68]Ga-citrate PET detects prostate cancer

Spencer C. Behr[1,*], **Rahul Aggarwal**[2,*], **Youngho Seo**[1], **Carina M. Aparici**[1], **Emily Chang**[2], **Kenneth T. Gao**[1], **Dora H. Tao**[1], **Eric J. Small**[2], and **Michael J. Evans**[1,#]

[1]Department of Radiology and Biomedical Imaging, University of California, San Francisco, 505 Parnassus Avenue, San Francisco, CA 94143

[2]Department of Medicine, University of California, San Francisco, 505 Parnassus Avenue, San Francisco, CA 94143

Abstract

Purpose: The management of advanced or recurrent prostate cancer is limited in part by the lack of effective imaging agents. Metabolic changes in prostate cancer have previously been exploited for imaging, culminating in the recent US-FDA approval of [11]C-choline for the detection of subclinical recurrent disease after definitive local therapy. Despite this milestone, production of [11]C-choline requires an onsite cyclotron, limiting the scope of medical centers at which this scan can be offered. In this pilot study, we tested whether prostate cancer could be imaged with positron emission tomography (PET) using [68]Ga-citrate, a radiotracer that targets iron metabolism but is produced without a cyclotron.

Procedures: Eight patients with castrate resistant prostate cancer were enrolled in this single center feasibility study. All patients had evidence of metastatic disease by standard of care imaging (CT, bone scan or MRI) prior to PET with [68]Ga-citrate. Patients were intravenously injected with increasing doses of ^{68}Ga-citrate (136.9 to maximum of 259 MBq). Uptake time was steadily increased from 1 hour to approximately 3.5 hours for the final 4 patients, and all patients were imaged with a PET/MRI. Qualitative and semi-quantitative (SUV_{max}) assessment of the metastatic lesions were performed and compared to standard of care imaging.

Results: At 1 and 2 hour imaging times post injection, there were no detectable lesions with [68]Ga citrate PET. At 3 to 4 hours uptake time, there were a total of 71 [68]Ga-citrate positive lesions (67 osseous, 1 liver, 3 lymph node). Of these, 65 lesions were visible on the standard of care imaging (CT and/or bone scan). 1 PET avid osseous vertebral body metastasis was not apparent on either CT or bone scan. Twenty five lesions were not PET avid but seen on CT and bone scan (17 bone, 6 lymph node, 1 pleural, and 1 liver). The average of the SUV_{max} values for bone or soft tissue metastases for patients treated at higher doses and uptake time was statistically

[#] To whom correspondences should be addressed. Corresponding author: Michael J. Evans, PhD, UCSF, Department of Radiology and Biomedical Imaging, 185 Berry Street, Lobby 6, Suite 350, San Francisco, CA 94107, michael.evans@ucsf.edu, Phone: 415-353-3442, Fax: 415-353-3592.

[*]These authors contributed equally to this work.

Conflicts of interest: M.J.E. receives consulting fees and owns shares in ORIC Pharmaceuticals, Inc. S.C.B receives consulting fees from GE Healthcare.

Informed consent: Informed consent was obtained from all individual participants included in the study.

higher than the corresponding parameter in normal liver, muscle and bone. Visually obvious blood pool activity was observed even 3–4 hours post injection, suggesting that further optimization of the [68]Ga-citrate imaging protocol is required to maximize signal-to-background ratios.

Conclusions: Our preliminary results support that PET with [68]Ga-citrate may be a novel tool for imaging prostate cancer. Future studies are needed to determine the optimal imaging protocol, the clinical significance of [68]Ga-citrate uptake, and its role in therapeutic decisions.

Introduction:

Despite intense research efforts, there are relatively few nuclear imaging tools that effectively detect prostate cancer. The current standard of care resources are [99m]Tc-MDP or HDP (methylene diphosphonate or hydroxymethylene diphosphonate), a radiotracer for either 2D-planar or SPECT that detects bone remodeling (the “bone scan”), [18]F-NaF, a radiotracer for PET that detects bone remodeling, and [11]C-choline, a radiotracer for PET that targets prostate cancer tumor cells[1–2].

All have recognized limitations. For instance, metabolic bone imaging agents are not specific for the microenvironment around osseous prostate cancer lesions, and will detect bone remodeling due to non-malignant pathologies (e.g. microfractures). Moreover, they do not detect soft tissue lesions, limiting its application in the substantial number of advanced prostate cancer patients with predominantly soft tissue/visceral metastases. Using bone scans to monitor the response of advanced prostate adenocarcinoma to systemic therapies is challenging because bone remodeling can persist for weeks or even months after ablation of the nearby tumor. [11]C-choline was recently approved for the detection of occult prostate cancer lesions in post-prostatectomy patients with rising serum PSA, and may prove to have applications in earlier or later stages of disease. While [11]C-choline targets the prostate cancer cell, and takes advantage of the technical virtues associated with PET, the short half-life of carbon-11 ($t_{1/2}$ ~20 min) restricts the use of this radiotracer to major medical centers that can afford an onsite cyclotron. Lastly, [18]F-FDG PET has limited sensitivity for detection of metastatic lesions (with the exception of rare, poorly differentiated visceral lesions), and is confounded by accumulated signal in the urinary collecting system.

An effective radiotracer for prostate cancer should detect both soft tissue and bony lesions, produce emissions compatible with PET for optimal resolution of disease foci, have a short radioactive and biological half-life to limit absorbed dose to the patient, and be widely available. Surveying the literature, we hypothesized that [68]Ga-citrate could satisfy these conditions. First, [67]Ga-citrate, an iron mimetic *in vivo*, has a longstanding history as an oncologic imaging agent, most notably for lymphoma, but also for certain solid tumors[3]. Among solid tumors, prostate cancer was disclosed in one report to harbor avidity for [67]Ga-citrate[4]. [68]Ga-citrate also behaves as an iron mimetic *in vivo*, suggesting it may also target prostate cancer lesions. Additionally, [68]Ga-citrate satisfies the aforementioned technical considerations, as it is compatible with PET, it clears quickly from the serum after binding to apo-transferrin, it has a short half-life ($t_{1/2}$ ~ 68 min), and gallium-68 is produced as a chloride salt from a commercial benchtop [68]Ge/[68]Ga generator rather than a cyclotron[5].

There is also a reasonable biological justification to argue for detecting prostate cancer with [68]Ga-citrate. Since gallium-68 binds to transferrin (Tf) in situ, the uptake of this radiotracer in tumors is a measurement of biologically active transferrin receptor (TFRC)[6]. Prostate cancer is broadly enriched in the lesions known to upregulate TFRC expression and activity (MYC and PI3K signaling), and on this basis, we hypothesize clinical disease may be generally avid for [68]Ga-Tf[7–8].

Collectively, these considerations led us to conduct the first feasibility study to test whether [68]Ga-citrate could demarcate prostate cancer tumors.

Materials and Methods

Patient selection

All patients had histologic evidence of prostate cancer with castration resistant disease by PCWG2 criteria[9]. Patients were required to have undergone standard clinical staging scans including a CT of the abdomen and pelvis with intravenous contrast and nuclear medicine bone scan ([99m]Tc-HDP) within 12 weeks prior to [68]Ga-citrate PET imaging. All patients had imaging evidence of metastatic disease by either CT or bone scan. The study was approved by the UCSF institutional review board (IRB), and all patients signed an informed consent form prior to [68]Ga-citrate scanning.

PET imaging protocol

All studies were performed on a SIGNA PET/MR scanner (GE Healthcare, Waukesha, WI). Patients were scanned after intravenous administration of [68]Ga-citrate. Three-dimensional PET data were acquired in list-mode with a 4 to 8 minute emission scan per bed for 6 bed stations. PET had 600 mm transaxial field of view (FOV) and 250 mm axial FOV. PET images were reconstructed with matrix size 128 × 128, 16 subsets and 4 iterations of time-of-flight enabled 3D ordered subset expectation maximization (TOF-3D-OSEM) algorithm, 8 mm full-width at half-maximum in-plane Gaussian post-reconstruction filter with a heavy z-axis filter as defined by the scanner manufacturer. Attenuation correction for PET reconstruction was performed using a MR-based attenuation correction (MRAC) technique provided by the scanner manufacturer.

Full body MR examination was performed without IV contrast. MRAC, 3D dual-echo, spoiled gradient echo sequence with two-echo based Dixon fat-water, axial T1 single-shot fast spin echo MR sequences were performed at each bed using the body surface coil.

Image Analysis

Maximum intensity projection (MIP), axial, coronal and sagittal reconstructions and PET/MR fused images were reviewed on an Advantage Windows Workstation (AW, Waukesha, WI). First, images were scored qualitatively for the presence of abnormal uptake by two experienced nuclear physicians (S.C.B., C.M.A.) on a score of 1 to 3, based on the following scoring scale:

1 = No lesions seen

2 = Fair, lesions seen, but noise/artifact-limited evaluated

3 = Adequate, lesions easily seen and assessed

Next, PET images were evaluated by a ABNM trained nuclear medicine physician with over 8 years of experience (S.C.B., C.M.A.) and scored for the presence of PET avid lesions. Lesions were considered PET positive if uptake was focal, greater than the adjacent background soft tissue and not in an expected physiologic structure such as the urinary bladder, vessels or salivary glands.

For semi-quantitative analysis, a volume of interest (VOI) was manually drawn around PET-avid lesions. The SUV_{max} and SUV_{mean} were recorded. The location of abnormal radiotracer uptake was compared to CT and bone scan. Additionally, SUV_{mean} and SUV_{max} were recorded in the liver, paraspinous soft tissues, bone (right sacrum), and mediastinal blood pool.

CT images were reviewed by an experienced, fellowship trained Abdominal Imaging radiologist with over 10 years of experience (S.C.B.) for the presence of metastases. Lymph nodes measuring ≥ 8 mm short axis in the iliac chain and ≥ 10 mm short axis for remainder of the abdominal and thoracic lymph nodes were used to define positive involvement by CT[10]. For non-nodal soft tissue lesions, measurements were recorded in long axis and considered positive if greater than 1 cm or clearly new from prior examinations when available. Nuclear medicine bone scans were reviewed by a nuclear medicine physician with over 10 years of experience (S.C.B., C.M.A.) and recorded the location of abnormal uptake.

Results

Eight patients were enrolled into this pilot study. The median age was 69 years old (59 to 79 years). All patients had castration resistant prostate cancer metastatic to the bone, and a subset had additional sites of disease including the lymph nodes (N = 4) and the liver (N = 1). Baseline patient characteristics are summarized in Table 1.

Table 2 summarizes the procedure and quality assessment for each PET examination. Patient 1 was injected with ~170 MBq of [68]Ga-citrate, and acquired PET data at 60 min and 120 min post injection. Despite evidence of lymph node lesions by CT and MRI, no tumor uptake of [68]Ga-citrate was observed. Significant blood pool activity was noted on the MIP. Collectively, these observations suggested that the dose and/or time of imaging post injection were too low for tumor detection.

Patients 2 and 3 were subsequently injected with the same dose of [68]Ga-citrate, and imaged at 180 and 210 minutes respectively. Although tumor uptake in skeletal lesions and in one liver metastasis was clear, the overall quality of the scans was still poorly scored. To further increase the signal to noise ratio, patient 4 was injected with a larger dose (~260 MBq) of [68]Ga-citrate and imaged at 225 min post injection. Two sclerotic bone lesions in the left femur were clearly resolved at 225 min, and the image quality was scored as “adequate” (Figure 1A). These lesions were also active on the bone scan (Figure 1B). Four additional patients (patient 5–8) were scanned using the same parameters. There was clear evidence of tumor uptake of [68]Ga-citrate in at least one lesion per patient, and all scans

were scored as at least “fair” (Table 3, and Supplemental Table 1; all imaging data are available upon request).

In this 8 patient cohort, a total of 96 lesions were detected with standard imaging scans, of which 84 were osseous and 12 were soft tissue (2 liver, 1 pleural, 9 lymph nodes). Four of the 8 patients had soft tissue metastases, 3 with lymph nodes, 1 liver, and 1 patient had both 1 lymph node and pleural metastases. There were 71 PET-avid lesions, of which 67 were osseous and 4 were soft tissue (1 liver, three lymph nodes). The average SUV_{max} for all lesions was 6.1 (SD = 2.2, range 2.9 to 14.9). Of the 67 PET-avid osseous lesions, 65 had corresponding findings on both CT and HDP bone scan, 1 did not have findings on either CT or bone correlate and 1 had HDP correlate, but no CT correlate. The one PET-avid lesion without CT or HDP correlate was in a T5 thoracic vertebral body in patient 3. Three areas of [68]Ga-citrate uptake corresponded to regions of presumed chronic inflammation based upon clinical history; (1) right glenohumeral joint (SUV_{max} = 1), (2) right greater trochanter bursa (SUV_{max} = 1.8) and (3) anal uptake (SUV_{max} = 3).

There were a total of 12 soft tissue metastases seen on CT imaging, of which 4 were PET positive, and 8 were PET negative. Of the 4 PET positive lesions, 1 was hepatic, 3 were lymph nodes (Figure 2). The average SUV_{max} of the soft tissue metastases was 8 (SD = 2.13, range 5.8 to 10.8). All of the lesions had a CT correlate with an average size of 1.8 cm (SD = 1.3, range 1 to 3.8). Of the 8 PET negative lesions, 6 were lymph node, 1 liver and 1 pleural with average CT size of 1.8 cm (SD = 0.5, range 1.3 to 2.6 cm). Finally, the average SUV_{max} of all soft tissue and osseous metastases from patients 4–8 was statistically greater than that of liver, muscle, and bone (Figure 3B). Blood pool activity was not statistically lower than the SUV_{max} of soft tissue or bony metastases ($P > 0.01$).

Discussion

In this study, we demonstrate that PET with [68]Ga-citrate can resolve soft tissue and bony metastatic prostate cancer lesions. Our data suggests that ≥ 210 MBq of [68]Ga-citrate, and ≥ 210 minutes of imaging time post injection, combined with a modern high-sensitivity PET scanner, are required for adequate quality images. At these thresholds, [68]Ga-citrate tumor uptake was generally congruent with lesion assignment by CT, MRI and bone scan, and SUV_{max} values for tumor lesions were consistently higher than that observed in TFRC-expressing normal tissues like muscle, liver, and bone. Lastly, our data shows that [68]Ga-citrate can detect prostate cancer embedded within historically challenging microenvironments like the liver and lymph nodes. These data suggest that [68]Ga-citrate may have utility in detecting early disease within pelvic lymph nodes, and assessing visceral tumor burden in advanced prostate cancer.

Despite the short half-life of gallium-68, we found that tumor imaging is possible using a relatively modest dose within four hours post injection using increasingly available high-sensitivity PET scanners. While noteworthy, this finding is consistent with previous studies of [18]F-labeled Tf in primates. Indeed, Eckelman and colleagues showed evidence of specific uptake of [18]F-Tf in healthy baboon livers within 30 minutes post injection[11–12]. Together, these observations underscore the unusually rapid delivery of Tf from the

blood to peripheral tissues with biologically active TFRC, and provide a potential mechanistic rationale for our data.

Although [68]Ga-citrate resolved many metastatic prostate cancer lesions, approximately 25% of lesions detected by bone scan or CT were not obviously identified with [68]Ga-citrate. In particular, only 4 of 10 lymph node metastases (40%) were detectable on [68]Ga-citrate PET. We are currently working to understand the basis for these observations. Because the blood pool activity was still significant using conditions that successfully highlight metastases, our leading hypothesis is that some prostate cancer metastases score as false negatives due to insufficient access to the radiotracer. We are currently testing this hypothesis more systematically. One additional consideration is that the undetected lesions may represent the minority of prostate cancer that does not harbor hyperactive MYC or PI3K signaling. Additionally, we observed low radiotracer uptake in the three areas that were felt to be inflammation, two related to osteoarthritis and one to proctitis. Overall, there were fewer areas of uptake attributable to osteoarthritis on [68]Ga-citrate PET than standard radionuclide bone scan. The true sensitivity and specificity of [68]Ga-citrate PET in patients with concurrent chronic inflammatory conditions will require further prospective evaluation.

There are several limitations to our study. First, it was limited by the small cohort size (n=8) as this was a proof of concept study. Additionally, the lack of pathologic confirmation and long-term follow up limits the assessment of false positive and negative findings. Therefore, larger scale studies as well as studies paired with biopsies and clinical follow up are warranted.

Many radiotracers have been evaluated in men with prostate cancer without finding a role in standard of care. Prominent examples include metabolic probes like 1-[11]C-acetate and 1-methyl-[11]C-methionine, 16-beta-[18]F-fluoro-5alpha-dihydrotestosterone, [18]F-choline, and various ligands to prostate specific membrane antigen (PSMA)[13–21]. Some tools like [11]C-acetate, [18]F-choline and [11]C-methionine have shown promise as lineage markers of prostate cancer, but it is not yet clear if they represent an improvement over [11]C-choline. 16-beta-[18]F-fluoro-5-alpha-dihydrotestosterone has been applied to patients with castration resistant prostate cancer to detect androgen receptor-positive disease, and quantify the pharmacodynamics effects of antiandrogens. That said, 16-beta-[18]F-fluoro-5-alpha-dihydrotestosterone cannot be used to detect prostate cancer in pre-castrate settings (abundant intratumoral androgens out-compete the radiotracer for androgen receptor binding), and this tool cannot be used to detect the growing percentage of androgen receptor-null, neuroendocrine like disease that emerges in castration resistant prostate cancer[22]. Antibodies and ligands to PSMA also will not detect neuroendocrine prostate cancer, though they may be very useful to detect micrometastases in early disease or measure the effects of antiandrogen therapy[23–24]. Some studies with [68]Ga-HBED CC have suggested PSMA PET outperforms both conventional imaging and [18]F-choline in the detection of recurrent subclinical disease[25–26]. While PSMA imaging is clearly promising, further work is needed to determine exactly where it and other agents fit in the prostate cancer treatment algorithm.

Conclusions

In this study we establish that prostate cancer metastases can be visualized with [68]Ga-citrate. Preliminary guidelines were defined for minimum dose and time post injection. Further study is warranted to determine the conditions required to visualize all metastases, or to establish more robustly if some lesions are inherently quiescent for this radiotracer. Moreover, the patient cohort will be increased to corroborate the findings of this feasibility study.

Supplementary Material

Refer to Web version on PubMed Central for supplementary material.

Acknowledgments:

We gratefully acknowledge Vahid Ravanfar for technical assistance, Dr. Jim Slater and the Cyclotron Core Facility at UCSF for the production of ^{68}Ga-citrate, and Drs. Randall Hawkins, Charles Ryan, John Kurhanewicz, Dan Vigneron, Sarah Nelson, and Henry VanBrocklin for constructive comments about the manuscript. M.J.E. was supported by the National Cancer Institute (R00CA172695, R01CA176671), and a Department of Defense Idea Development Award (PC140107). M.J.E. and R.A. are Prostate Cancer Foundation Young Investigators. M.J.E., R.A. and S.C.B. were supported by the UCSF Academic Senate Committee on Research. Y.S. was supported by the National Cancer Institute (R01CA154561).

References:

1. Kiess AP, Cho SY, Pomper MG (2013) Translational Molecular Imaging of Prostate Cancer. Current radiology reports 1:216–226. [PubMed: 24159427]
2. Hara T, Kosaka N, Kishi H (1998) PET imaging of prostate cancer using carbon-11-choline. Journal of nuclear medicine : official publication, Society of Nuclear Medicine 39:990–995.
3. Cai J, Li F (2013) Single-photon emission computed tomography tracers for predicting and monitoring cancer therapy. Current pharmaceutical biotechnology 14:693–707. [PubMed: 24372237]
4. Sauerbrunn BJ, Andrews GA, Hubner KF (1978) Ga-67 citrate imaging in tumors of the genito-urinary tract: report of cooperative study. Journal of nuclear medicine : official publication, Society of Nuclear Medicine 19:470–475.
5. Banerjee SR, Pomper MG (2013) Clinical applications of Gallium-68. Applied radiation and isotopes : including data, instrumentation and methods for use in agriculture, industry and medicine 76:2–13.
6. Larson SM, Rasey JS, Allen DR, et al. (1980) Common pathway for tumor cell uptake of gallium-67 and iron-59 via a transferrin receptor. Journal of the National Cancer Institute 64:41–53. [PubMed: 6243376]
7. Robinson D, Van Allen EM, Wu YM, et al. (2015) Integrative clinical genomics of advanced prostate cancer. Cell 161:1215–1228. [PubMed: 26000489]
8. Taylor BS, Schultz N, Hieronymus H, et al. (2010) Integrative genomic profiling of human prostate cancer. Cancer cell 18:11–22. [PubMed: 20579941]
9. Scher HI, Halabi S, Tannock I, et al. (2008) Design and end points of clinical trials for patients with progressive prostate cancer and castrate levels of testosterone: recommendations of the Prostate Cancer Clinical Trials Working Group. Journal of clinical oncology : official journal of the American Society of Clinical Oncology 26:1148–1159. [PubMed: 18309951]
10. Koh DM, Hughes M, Husband JE (2006) Cross-sectional imaging of nodal metastases in the abdomen and pelvis. Abdominal imaging 31:632–643. [PubMed: 16897278]

11. Aloj L, Carson RE, Lang L, Herscovitch P, Eckelman WC (1997) Measurement of transferrin receptor kinetics in the baboon liver using dynamic positron emission tomography imaging and [18F]holo-transferrin. Hepatology 25:986–990. [PubMed: 9096608]
12. Aloj L, Lang L, Jagoda E, Neumann RD, Eckelman WC (1996) Evaluation of human transferrin radiolabeled with N-succinimidyl 4-[fluorine-18](fluoromethyl) benzoate. Journal of nuclear medicine : official publication, Society of Nuclear Medicine 37:1408–1412.
13. Mari Aparici C, Seo Y (2012) Functional imaging for prostate cancer: therapeutic implications. Seminars in nuclear medicine 42:328–342. [PubMed: 22840598]
14. Nunez R, Macapinlac HA, Yeung HW, et al. (2002) Combined 18F-FDG and 11C-methionine PET scans in patients with newly progressive metastatic prostate cancer. Journal of nuclear medicine : official publication, Society of Nuclear Medicine 43:46–55.
15. Morris MJ, Akhurst T, Osman I, et al. (2002) Fluorinated deoxyglucose positron emission tomography imaging in progressive metastatic prostate cancer. Urology 59:913–918. [PubMed: 12031380]
16. Beattie BJ, Smith-Jones PM, Jhanwar YS, et al. (2010) Pharmacokinetic assessment of the uptake of 16beta-18F-fluoro-5alpha-dihydrotestosterone (FDHT) in prostate tumors as measured by PET. Journal of nuclear medicine : official publication, Society of Nuclear Medicine 51:183–192.
17. Pandit-Taskar N, O'Donoghue JA, Durack JC, et al. (2015) A Phase I/II Study for Analytic Validation of 89Zr-J591 ImmunoPET as a Molecular Imaging Agent for Metastatic Prostate Cancer. Clinical cancer research : an official journal of the American Association for Cancer Research 21:5277–5285. [PubMed: 26175541]
18. Oyama N, Akino H, Kanamaru H, et al. (2002) 11C-acetate PET imaging of prostate cancer. Journal of nuclear medicine : official publication, Society of Nuclear Medicine 43:181–186.
19. Kiess AP, Banerjee SR, Mease RC, et al. (2015) Prostate-specific membrane antigen as a target for cancer imaging and therapy. The quarterly journal of nuclear medicine and molecular imaging : official publication of the Italian Association of Nuclear Medicine 59:241–268.
20. Marzola MC, Chondrogiannis S, Ferretti A, et al. (2013) Role of 18F-choline PET/CT in biochemically relapsed prostate cancer after radical prostatectomy: correlation with trigger PSA, PSA velocity, PSA doubling time, and metastatic distribution. Clinical nuclear medicine 38:e26–32. [PubMed: 23242060]
21. Chondrogiannis S, Marzola MC, Grassetto G, et al. (2015) Optimized protocol for (18)F-choline PET/CT in patients with biochemically relapsed prostate cancer: experiences on 250 consecutive cases. Clinical nuclear medicine 40:e308–312. [PubMed: 25742236]
22. Beltran H, Prandi D, Mosquera JM, et al. (2016) Divergent clonal evolution of castration-resistant neuroendocrine prostate cancer. Nature medicine.
23. Evans MJ, Smith-Jones PM, Wongvipat J, et al. (2011) Noninvasive measurement of androgen receptor signaling with a positron-emitting radiopharmaceutical that targets prostate-specific membrane antigen. Proceedings of the National Academy of Sciences of the United States of America 108:9578–9582. [PubMed: 21606347]
24. Evans MJ (2012) Measuring oncogenic signaling pathways in cancer with PET: an emerging paradigm from studies in castration-resistant prostate cancer. Cancer discovery 2:985–994. [PubMed: 23043150]
25. Afshar-Oromieh A, Zechmann CM, Malcher A, et al. (2014) Comparison of PET imaging with a (68)Ga-labelled PSMA ligand and (18)F-choline-based PET/CT for the diagnosis of recurrent prostate cancer. European journal of nuclear medicine and molecular imaging 41:11–20. [PubMed: 24072344]
26. Giesel FL, Fiedler H, Stefanova M, et al. (2015) PSMA PET/CT with Glu-urea-Lys-(Ahx)-[(6)(8)Ga(HBED-CC)] versus 3D CT volumetric lymph node assessment in recurrent prostate cancer. European journal of nuclear medicine and molecular imaging 42:1794–1800. [PubMed: 26162799]

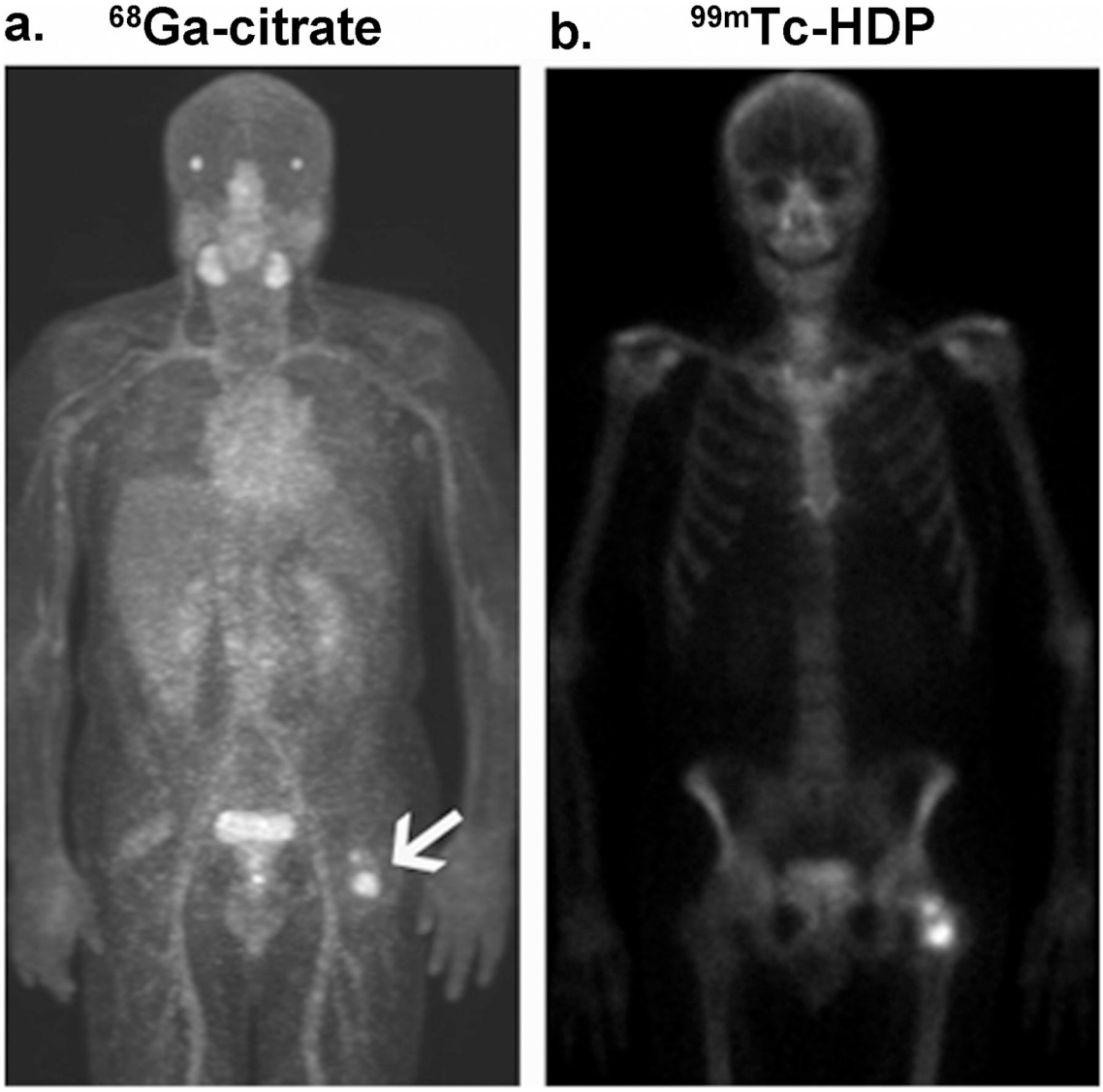

Figure 1. Representative ^{68}Ga-citrate images showing detection of skeletal metastases.

A. A MIP collected 210 minutes post injection shows two sclerotic bone lesions in the left femur (white arrow) are avid for ^{68}Ga-citrate in patient 4. **B.** The ^{99m}Tc-MDP scan shows the corresponding skeletal tumor burden.

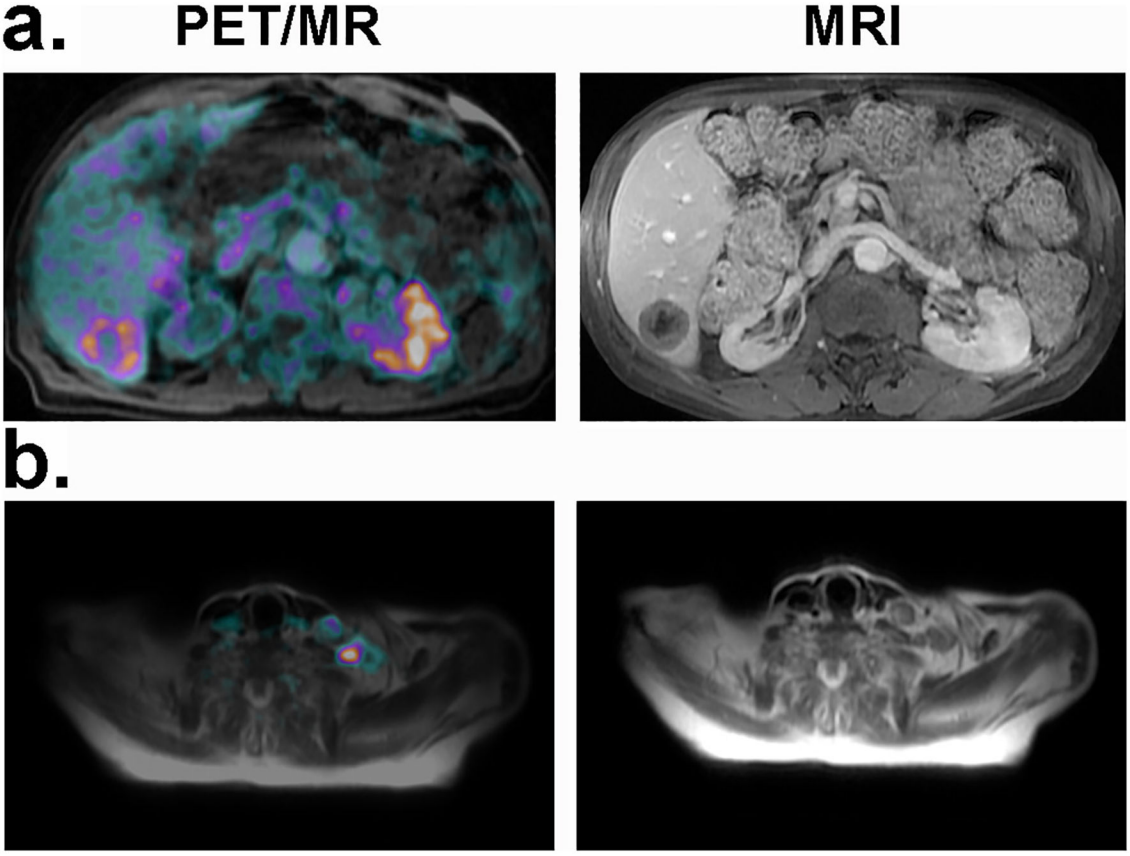

Figure 2. ^{68}Ga-citrate demarcates soft tissue lesions.

A. PET/MR and MR slices highlighting a necrotic liver metastasis from patient 3. The SUV_{max} of the liver metastasis was 5.2, above blood pool (3.8), normal liver (3.5), muscle (1.2), and bone (2.2). B. PET/MR and MR slices highlighting a supraclavicular lymph node metastasis from patient 8. The SUV_{max} was 10.8, above the blood pool (5.7), normal liver (4.3), muscle (2.0), and bone (1.9).

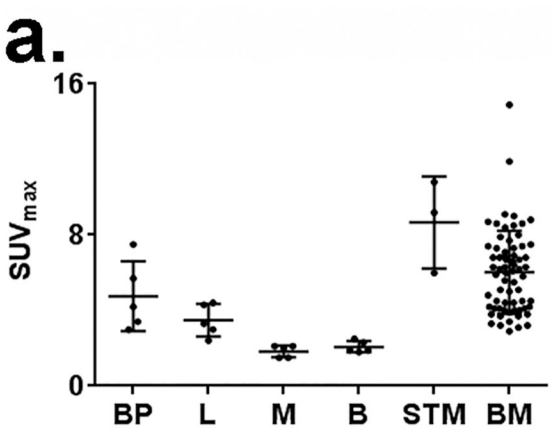

b.

	Bone metastasis	Soft Tissue Metastasis
Blood Pool	0.10	<0.05
Liver	<0.001	<0.001
Muscle	<0.001	<0.001
Bone	<0.001	<0.001

Figure 3. A summary of the SUV_{max} data from patients 4–8.

A. A graphical representation of the SUV_{max} for blood pool (BP), liver (L), muscle (M), bone (B), soft tissue metastases (STM), and bone metastases (BM). **B.** A grid system showing the *P* value for soft tissue and bony metastases compared to the respective normal tissue for patients 4–8. All comparisons achieved statistical significance with the exception of that between blood pool and the respective pool of SUV_{max} data from metastases.

Table 1.

Patient characteristics

Characteristic	
Median age (range)	70 (59–79)
Gleason grade at diagnosis	
7	2 (25%)
≥ 8	6 (75%)
Median PSA, ng/mL (range)	37.7 (4.9–422)
Median LDH, units/L (range)	177.5 (118–397)
Median alkaline phosphatase, units/L (range)	101 (34–378)
Median hemoglobin, g/dL (range)	13.0 (8.2–15.6)
Sites of metastases	
Bone	8 (100%)
Node	4 (50%)
Liver	1 (13%)
Prior treatment for metastatic prostate cancer	
Primary androgen deprivation therapy	8 (100%)
Abiraterone	1 (13%)
Enzalutamide	2 (25%)
Both	5 (63%)
Neither	0

Table 2.

A summary of PET technique and quality assessment.

Patient #	Dose (MBq)	Uptake time	Time per bed	Quality
1	173.9	60, 120	4	1
2	136.9	180	5	1.5
3	210.9	210	8	1.5
4	259	225	8	3
5	262.7	210	8	2
6	259	210	8	3
7	259	240	8	2
8	203.5	210, 240	5	3

Table 3.

A summary of SUV_{max} and SUV_{mean} for normal soft tissues

Location	SUV_{max}			SUV_{mean}		
	Average	SD	Range	Average	SD	Range
Blood pool	5.0	1.9	3 – 8.2	4	1.2	2.5 – 6.3
Liver	3.5	1.0	2.4 – 5	2.2	0.6	1.4 – 3.3
Paraspinus	1.6	0.4	0.9 – 2.1	1	0.5	0.4 – 2
Right sacrum	2.0	0.6	0.8 – 2.5	1.1	0.4	0.5 – 1.7